SURFACE AND INTERFACE ANALYSIS
Surf. Interface Anal. 2005; **37**: 273–280
Published online 31 January 2005 in Wiley InterScience (www.interscience.wiley.com). DOI: 10.1002/sia.2015

SIA

Evolution of the local structure in GaN:O thin films grown by ion-assisted deposition with film thickness

M. J. Ariza,[1]* A. Koo,[2] H. J. Trodahl,[2] B. J. Ruck,[2] A. Bittar,[3] D. J. Jones,[4] B. Bonnet,[4] J. Rozière[4] and J. Moscovici[5]

[1] Grupo de Física de Fluidos Complejos, Departamento de Física Aplicada, Universidad de Almería, E-04120 Almería, Spain
[2] School of Chemical and Physical Sciences, Victoria University of Wellington, PO Box 600, Wellington, New Zealand
[3] Industrial Research Ltd, PO Box 31310, Lower Hutt, New Zealand
[4] Laboratoire des Agrégats Moléculaires et Matériaux Inorganiques, UMR CNRS 5072, Université Montpellier II, Place Eugène Bataillon, F-34095 Montpellier Cédex 5, France
[5] Groupe de Physique des Milieux Denses, UFR Sciences et Technologie, Universite Paris XII-Val de Marne, 61 Avenue du General de Gaulle, F-94010 Creteil Cédex, France

Received 2 April 2004; Revised 16 October 2004; Accepted 19 October 2004

Optical and optoelectronic properties of gallium nitride strongly depend on the synthesis procedure, which may be related to specific structural characteristics of GaN inherent to each preparation condition. Amorphous and nanocrystalline GaN films have been prepared by ion-assisted deposition (IAD). The films prepared at 10^{-5} Torr for <50 min have shown exploitable optoelectronic properties, in spite of the high concentration of oxygen of these films (up to 25 at.%). We study here the evolution of the local structure around Ga atoms as the deposition time increases. Five IAD GaN films of thickness ranging between 140 and 450 nm on silicon substrates were analysed by x-ray absorption fine structure (XAFS) at the Ga K-edge. The first and second shells of neighbouring atoms are clearly identified in the radial distribution functions at approximately 1.9 and 3.2 Å, respectively. In all of the films, Ga seems to be tetrahedrally coordinated to four nitrogen atoms, some of which may be substituted by oxygen. For deposition times <50 min, analysis of both x-ray adsorption near-edge structure (XANES) and extended x-ray adsorption fine structure (EXAFS) regions indicates that the material is highly amorphous. Above this threshold, a peak corresponding to the first coordination sphere of Ga atoms becomes discernible and increases in intensity for longer deposition times, indicating that the second shell of atoms is now more ordered. The pseudo Debye–Waller factor of the Ga shell is used for monitoring the average degree of amorphization in an ∼100 nm thick top layer, which seems to be related to the film oxygen content. The XAFS results are compatible with a layered distribution of crystallinity, as has been suggested previously for these films.

KEYWORDS: total electron yield XAFS; gallium nitride; Ga K-edge EXAFS; ion-assisted deposition

INTRODUCTION

Epitaxial deposition of crystalline gallium nitride (x-GaN) is extremely difficult due to a lack of suitable lattice matches that minimize dislocations at the GaN/substrate interface. Amorphous gallium nitride (a-GaN) has been suggested as an alternative to x-GaN for developing green-blue-UV optoelectronic devices.[1] Fully a-GaN seems to have a well-defined bandgap close to that of x-GaN and is reasonably free of midgap states.[1,2] But the amorphous state is not in itself unique and each preparation method may have specific local structural characteristics.[3,4] It has been shown also that optoelectronic properties depend on the details of the nanostructure. Although different attempts to explore a-GaN have been reported already,[2,5–17] relationships between electronic properties and the atomic bonding configuration have not yet been clearly established.

Amorphous GaN materials have been synthesized using reactive sputtering of a Ga target in a nitrogen atmosphere[18,19] by implantation of Ga ions into different nitride substrates,[20,21] and also using molecular beam epitaxy.[6] Residual oxygen is a common impurity of polycrystalline GaN films, which also alters the film electrical properties.[22,23] Oxygen is assumed to substitute for nitrogen in GaN, forming an oxynitride solid solution (GaN:O) that may accommodate up to 25 at.% of oxygen without substantially altering the tetrahedral configuration of Ga atoms.[23–25] The presence of oxygen in GaN seems to promote the formation of Ga vacancies[22] and to stabilize the long-range amorphous structure.[25,26]

We have prepared nanocrystalline and amorphous GaN films on a wide variety of substrates by ion-assisted

*Correspondence to: M. J. Ariza, Grupo de Física de Fluidos Complejos, Departamento de Física Aplicada, Universidad de Almería, E-04120 Almería, Spain. E-mail: mjariza@ual.es
Contract/grant sponsor: MCyT.

deposition (IAD).[9] This method provides homogeneous films with a good control of the stoichiometry over a wide range of thicknesses.[27] To obtain the IAD films, Ga atoms are evaporated inside a vacuum chamber and an energetic beam of nitrogen ions provides a convenient route to overcome energy barriers to reaction. Stoichiometric nanocrystalline GaN with <1 at.% of oxygen impurities have been prepared working at a base pressure of 10^{-8} Torr.[26] To prepare amorphous films, the water-vapour partial pressure should be increased up to 10^{-5} Torr, giving films containing up to 20 at.% of oxygen for deposition times of <50 min.[28] Chemical, structural and optical properties of these films have been reported already[12–15] and the optoelectronic properties have been correlated with their nanostructure.[16] The objective of this work is to study possible changes on the local structure around Ga atoms as the film increases in thickness. Five GaN:O films were deposited onto crystalline silicon wafers under the same initial conditions and increasing deposition times (t_d). The film thickness corresponding to each t_d was estimated by reflectance and transmittance measurements.[9]

X-ray absorption fine structure (XAFS) is a powerful technique to study the local structure around a central atom.[29,30] In particular, coordination numbers and interatomic distances can be obtained from the extended x-ray absorption fine structure (EXAFS), which includes the energy region from ~30 to several hundred electron-volts above the atomic x-ray absorption edge. The fine structure in the near-edge region (XANES, within ~30 eV of the edge) is related to the density of unoccupied states and medium and long-range crystalline order. X-ray absorption fine structure is an interference phenomenon so local that oscillations are observed even in liquid materials.[31] X-ray absorption at the Ga K-edge has been used for characterizing the local structure of different types of GaN materials. Among others, Perlin *et al*. studied crystalline gallium nitride under pressure in transmission mode.[32] Katsikini *et al*. reported fluorescence EXAFS measurements on cubic and hexagonal GaN films.[33] Other epitaxial layers, as well as a crystalline bulk GaN sample with the wurtzite structure, were analysed by Lawniczak-Jablonska *et al*. using total electron yield EXAFS.[34] Li *et al*. studied both nanocrystalline (average grain size of 12 nm) and monocrystalline GaN.[35]

Here, we use XAFS at the gallium K-edge to study GaN films that are fully amorphous or nanocrystalline (grain size ~3 nm) as seen by both x-ray and electron diffraction. Because samples are relatively thin films deposited on the top of thick substrates, an indirect method with high surface sensitivity must be used. The probed depth at the Ga K-edge using the total electron yield (TEY) method is of the order of tens nanometres[34,36–38] and the reliability of TEY XAFS for studying thin films and surfaces has been demonstrated already by comparison with transmission and fluorescence XAFS measurements, which are bulk sensitive.[36] Besides the IAD-grown GaN films, a polycrystalline GaN sample was used here as reference. This sample was studied in both TEY and transmission modes, to evaluate also the reliability of indirect TEY measurements.

EXPERIMENTAL

Sample preparation

Disordered GaN:O films were grown on Si(100) by ion-assisted deposition (IAD GaN films); Ga atoms are evaporated over the substrate in a vacuum chamber with a base pressure of 10^{-5} Torr (mainly water vapour) and simultaneously high-energy nitrogen ions are produced by a Kaufmann source. Both the ion energy and flux have been optimized to achieve a Ga:N ratio within 10% of unity.[13] All the films used in this work were prepared using 500 eV N ions and a flux of a few times that of the Ga atoms. The film grows on the surface of the substrate at a rate of ~0.5 Å s^{-1}. Five thin films of IAD GaN, named GaN*xx* (where $xx = 10$, 28, 30, 40 and 80 is the deposition time (t_d) in s 100^{-1}), were prepared (see Table 1). Film thickness (x_{opt}) was determined on films deposited on quartz in the range 200–1200 nm by optical transmittance and reflectance measurements,[9] which allow simultaneous determination of the film thickness and refractive index. The accuracy of the computed values of optical thickness was confirmed by transmission electron microscopy (TEM).[16]

Compositional and structural characterization of the IAD GaN films

Chemical composition of IAD GaN films has been determined by combined Rutherford backscattering spectroscopy (RBS) and nuclear reaction analysis.[28] The RBS results (Table 1) show a high oxygen content in the films grown for short times (<50 min). Long-range structural properties of some of these films also have been studied by resonant Raman spectroscopy, x-ray diffraction (XRD), TEM and electron diffraction.[13,16,39] Thin films (~140 nm) are amorphous, whereas films above ~400 nm thick give diffraction peaks of a width indicating nanocrystallites of ~3 nm. The local structures around N atoms of two films 140 and 400 nm thick were characterized by x-ray absorption near the nitrogen K-edge.[15,16,40] Results have showed that a film 150 nm thick is amorphous and has significant amounts of trapped molecular nitrogen, whereas local crystalline order is higher and the amount of N_2 is lower in a 400 nm thick film. In a preliminary study, x-ray absorption spectra at the Ga K-edge in transmission mode were recorded also on a thicker film (~1000 nm) deposited onto Mylar,[13] from which data it was concluded that IAD GaN films are predominantly heteropolar bonded with a local tetrahedral configuration. Defects consist of 5–20% of oxygen and some molecular N_2, but to

Table 1. Deposition time (t_d), optical thickness (x_{opt}), composition and long-range structure of IAD-grown GaN films

Sample	t_d (s)	x_{opt} (nm)	RBS (Ga:N:O)	Long-range structure (XRD crystallite size)
GaN10	1000	140	45:30:25	Amorphous (<1 nm)
GaN28	2800	150	(O > 20%)	Amorphous (<1 nm)
GaN30	3000	260	44:48:8	—
GaN40	4000	280	50:40:10	—
GaN80	8000	446	46:44:10	Nanocrystalline (~3 nm)

this stage of characterization we have no evidence of the existence of a separate metallic or gallium oxide phase.

X-ray absorption spectroscopy

X-ray absorption spectroscopy in total electron yield mode (TEY XAFS) was carried out using the spectrometer EXAFS-13, line D42 of the DCI storage ring at LURE (Paris Sud University). Synchrotron radiation and an Si[111] channel-cut monochromator were used for recording the spectra from 100 eV below to 1000 eV above the Ga K-edge (10 367 eV), the energy step being 2 eV in the EXAFS region. Energy was calibrated using a standard Zn foil by assigning $E_0 = 9659$ eV to the first point of inflection of the Zn K-edge. Samples were fixed to a stainless-steel support using conductive Ag paste. The TEY experiments were performed near the liquid nitrogen temperature (77 K) using a TEY detector designed at LURE.[41] X-ray absorption spectra ($\mu(E)$) are determined from the ratio of the TEY current (I_1) and the incident photocurrent (I_0) provided by an ionization chamber. The x-ray absorption spectrum of a powder reference sample supplied by Aldrich (wurtzite GaN, wGaN) was also recorded in transmission mode using a second ionization chamber after the sample.

Experimental data were analysed using the software developed by Michalowicz.[42] The same protocol was used for analysing all of the x-ray absorption experimental spectra, which includes: extraction of the EXAFS signal after subtraction of absorption of the central atom in the absence of neighbouring atoms ($\chi(k) = (\mu - \mu_1)/(\mu_1 - \mu_0)$), where the background before the edge (μ_0) was determined by linear fitting and μ_1 beyond the edge was modelled by a cubic spline with division of the spectrum into three equidistant zones; calculation of the pseudo radial distribution function $F(R)$ by fast Fourier transformation over the range 3–13 Å^{-1} and k^3 weighting; filtering of different coordination spheres in $F(R)$ and back-Fourier transformation to derive partial components of the EXAFS oscillations; and multivariate least-squares fitting of filtered $\chi(k)$ and $F(R)$ using calculated photoelectron phase and amplitude functions.[43]

RESULTS AND DISCUSSION

Reliability of the TEY EXAFS

A polycrystalline GaN sample (wGaN) was used to assess the reliability of our indirect TEY measurements. Figure 1 compares transmission and TEY EXAFS spectra (top) and the modulus of the pseudo radial distribution functions ($|F(R)|$, bottom), where the successive shells of atoms are marked 1–6. As can be observed, both detection methods give the same oscillation pattern, although the TEY amplitude is slightly smaller. This brings a fall of peak intensities of the second and successive shells in $|F(R)|$. On the other hand, the TEY spectrum has a poorer signal-to-noise ratio for $k > 10$ Å^{-1} due to the weak electronic current given in this mode of detection.

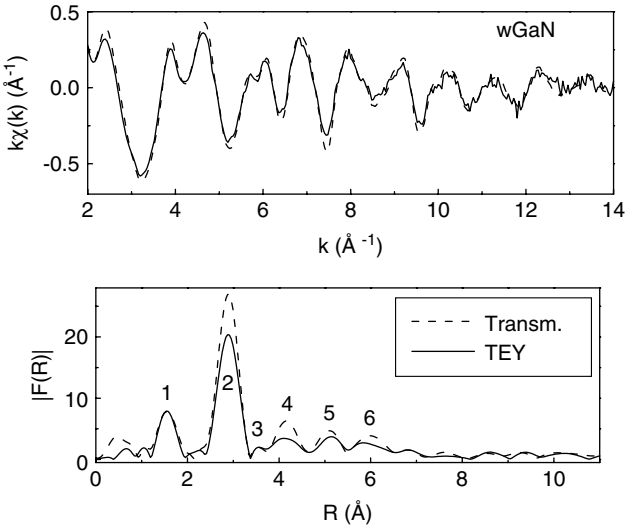

Figure 1. Comparison of EXAFS spectra of the polycrystalline wGaN recorded in transmission (dashed line) and TEY (solid line) mode (top) and modulus of the corresponding pseudo radial distribution function (bottom).

In contrast to zinc blende GaN (cubic symmetry, F43m space group),[44] in wurtzite GaN (hexagonal symmetry, P63mc space group) different types of atoms must contribute to each of the shells marked in Fig. 1 (bottom). However, the actual radial distribution of atoms can be simplified if atoms of each type at close but not identical distances are grouped in a single shell. This minimizes the number of fitting parameters to get a satisfactory fitting of the EXAFS spectra. Table 2 summarizes simplified interatomic distances (R_i) and the number and type of atoms (N_i(X), where X = N, Ga) of the successive shells for hexagonal (W-GaN) and cubic GaN (ZB-GaN).[44–46] Under these assumptions,

Table 2. Ideal interatomic distances (Å) of wurtzite GaN (wGaN) and zinc blende GaN (ZB-GaN) and interatomic distances (Å) and pseudo Debye–Waller factors (Å) of polycrystalline wGaN determined from transmission (Trans.) and TEY XAFS (TEY)

	R_1	N_1	R_2	N_2	R_3	N_3	R_{4a}	N_{4a}	R_{4b}	N_{4b}
W-GaN (P63mc)[a,b]	1.944	4 (N)	3.175	12 (Ga)	3.676	10 (N)	4.490	6 (Ga)	4.532	6 (N)
ZB-GaN (F-43m)[a,c]	1.931	4 (N)	3.154	12 (Ga)	3.698	12 (N)	4.460	6 (Ga)	—	—
wgaN	R_1	σ_1	R_2	σ_2	R_3	σ_3	R_{4a}	σ_{4a}	R_{4b}	σ_{4b}
Trans.	1.938	0.046	3.177	0.064	3.680	0.055	4.485	0.079	4.525	0.061
TEY	1.943	0.052	3.175	0.067	3.680	0.066	4.485	0.083	4.528	0.056

[a] Ideal crystallographic structure determined using Ref. 46.

[b] Lattice constants: $a = 3.192$ Å, $c = 5.196$ Å.[45]

[c] Lattice constant: $a = 4.46$ Å.[44]

interatomic distances and number of nearest neighbours around a central Ga atom are almost coincident in cubic and hexagonal structure up to the fourth shell. Thus, previous attempts to distinguish between cubic and hexagonal GaN by EXAFS at the Ga K-edge were unsuccessful.[33] However, these symmetries have been reported to show differential characteristics in the XANES region of the N K-edge,[47] and a shift towards high energies of the main XANES features at the Ga K-edge have also been assigned to a hexagonal to cubic transition in crystalline GaN.[32]

The structural parameters of wGaN can be refined from partial components of the EXAFS spectra. In the fitting procedure, partial filtered spectra were firstly fitted with a variable photoelectron mean free path, and a fixed scale factor S_0^2 of 0.8. The number of neighbours (N_i) was fixed to crystallographic values; thus the pseudo Debye–Waller factors (σ_i) accommodate small differences in distances. In this way, the photoelectron mean free path (γ_i), interatomic absorber–neighbour distance (R_i) and Debye–Waller factor (σ_i) of each shell were refined to obtain the best fit between experimental and simulated data. Initial values of the number of neighbours and interatomic distances were those indicated in Table 2 for W-GaN. The fitting residue was <2% in all cases. Figure 2 compares experimental (dots) and simulated (solid lines) EXAFS (top) and $|F(R)|$ (bottom) filtered up to the fourth shell from transmission and TEY spectra. Good agreement between experimental and calculated data is observed in both representations. Interatomic distances obtained from both spectra are very close to that of the ideal hexagonal structure (see Table 2). Differences are within expected experimental errors. The pseudo Debye–Waller factors are also very similar, but they are systematically smaller for transmission spectra.

Although the signal-to-noise ratio of TEY EXAFS spectra may reduce the exploitable k range, this experimental method is able to give structural parameters that are as reliable as those by transmission mode, and we have used it to study our IAD GaN films. The probed depth by TEY in nitride materials at photon energies close to 10^4 eV is <100 nm.[32–35] All the studied GaN films are thicker than 100 nm, and contribution of the substrate/GaN interface may be considered negligible.

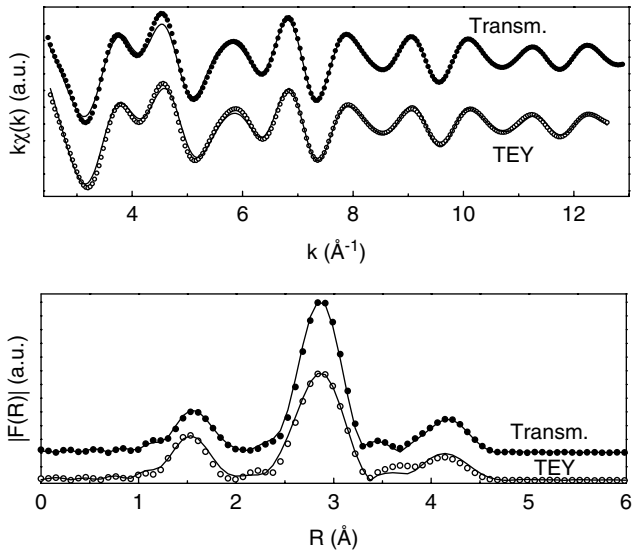

Figure 2. Fourth-shell filtered EXAFS (top) and modulus of the pseudo radial distribution function (bottom) extracted from transmission and TEY wGaN spectra. Comparison of experimental (symbols) and simulated (solid lines) data.

Local structure of the GaN : O films grown by IAD

In the IAD method, the film thickness is controlled by the deposition time. However, the growth rate may be different at different times during growth, because it is a fine balance between deposition rate and re-sputtering rate, which may depend on the presence of residual oxygen, for example. As can be observed in Table 1, there is no correlation between thickness and deposition time of GaN10 and GaN28, suggesting a sudden increase of the growth rate between 45 and 50 min of deposition, just when the oxygen content falls from 20 to 10 at.%. Despite this and assuming a constant growth rate, the linear fitting of optical thickness (x_{opt}) versus deposition time shows an average growth rate of 0.5 Å s^{-1} in all the films deposited at 10^{-5} Torr. Although this growth rate is very important for the preparation set-up, the actual thickness of most of the films is closer to x_{opt} than to the expected thickness at this average growth rate, as has been confirmed by TEM.

The near-edge region of x-ray absorption spectra of the five IAD GaN films and wGaN are plotted in Fig. 3. Spectra have been normalized to the same edge jump and shifted in the vertical axis to compare the edge shape. Despite the experimental conditions not being optimised for XANES analysis (energy resolution is not better than 1 eV), we can get some conclusions for this part of the spectra. Features on the edge and XANES region are related to the distribution of Ga and N p-states in the conduction band and to medium- and long-range structure. The edge inflection point is at 10 369 eV for wGaN and the thicker films, and it shifts slightly (<1 eV) to higher energies for GaN28 and GaN10. This indicates that the chemical environment of Ga atoms of the IAD GaN is very similar to that of wGaN. Both main features (A and B in Fig. 3) in the XANES region beyond the

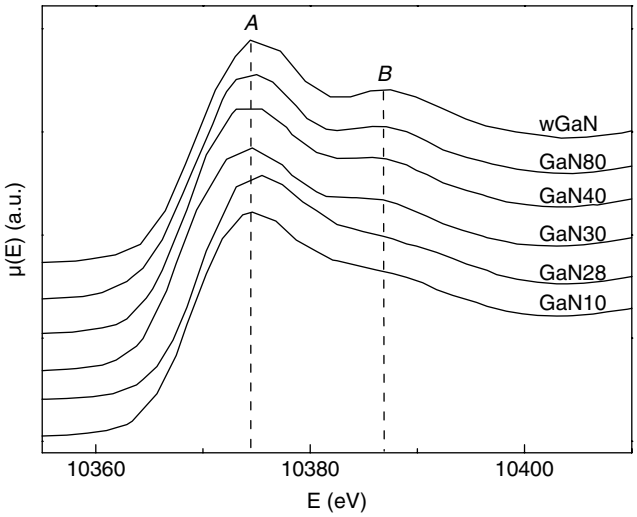

Figure 3. Near-edge region of the TEY x-ray absorption spectra of GaN10, GaN28, GaN30, GaN40, GaN80 and wGaN.

edge also shift slightly (<1 eV) to higher energies for thinner films (GaN28 and GaN10), which may be due to an increase in the percentage of nitrogen atoms substituted by oxygen atoms.

The energy gap between A and B is 11 eV for all of the samples, as in our reference wurtzite sample. This gap increases up to 18 eV for cubic GaN,[32] therefore the local structure of the IAD films is mainly hexagonal. The first peak (A) is at ~10 375 eV for all of the films and the wGaN reference sample. The same energy has been reported in the literature for the 1s to 4p transition of Ga tetrahedrally coordinated to oxygen,[48] which shifts 4 eV to higher energies for Ga octahedrally coordinated to oxygen atoms.[48] Because in the IAD GaN films the gap between A and B is much longer (11 eV), we identify peak B as the scattering resonance within the second coordination shell, as Dalba *et al*. have proposed for GaAs.[49] The intensity of B decreases at shorter deposition times and nearly disappears for GaN28 and GaN10, indicating an increase of structural disorder around Ga atoms.

In summary, analysis of the XANES region indicates that Ga is tetrahedrically coordinated mainly to N atoms in all of the films. Some nitrogen seems to be substituted by oxygen, mainly in thinner films. In the medium and long range, GaN tetrahedra prefer to order in a hexagonal symmetry (W-GaN).

Figure 4 plots the extracted EXAFS spectra of the IAD GaN films and the reference sample. The oscillation pattern of the thickest film is very similar to that of wGaN and other GaN EXAFS spectra in the literature.[35–38] For thinner films, the oscillations are dampened, which is characteristic of an increase of local disorder. The modulus of pseudo radial distribution functions (Fig. 5) shows a strong decrease of the second peak height with respect to wGaN. In the thinner films (GaN10 and GaN28) this shell cannot be distinguished from background noise, whereas the intensity of the first shell is almost the same for all the IAD GaN films and is only slightly lower than that of the reference sample. This shows the amorphous nature of the IAD GaN films for

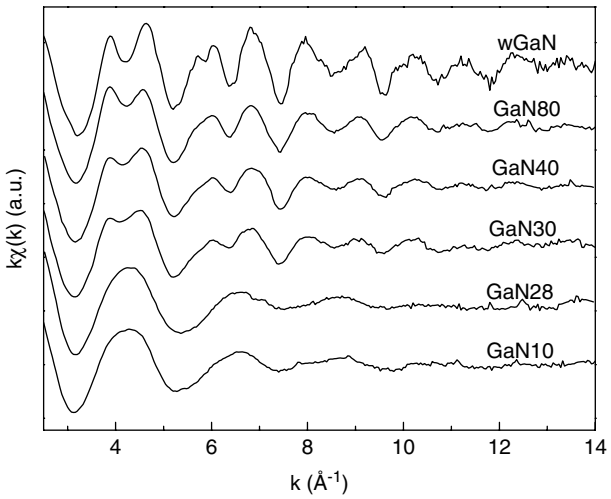

Figure 4. The EXAFS oscillations extracted from TEY x-ray absorption spectra of GaN10, GaN28, GaN30, GaN40, GaN80 and wGaN.

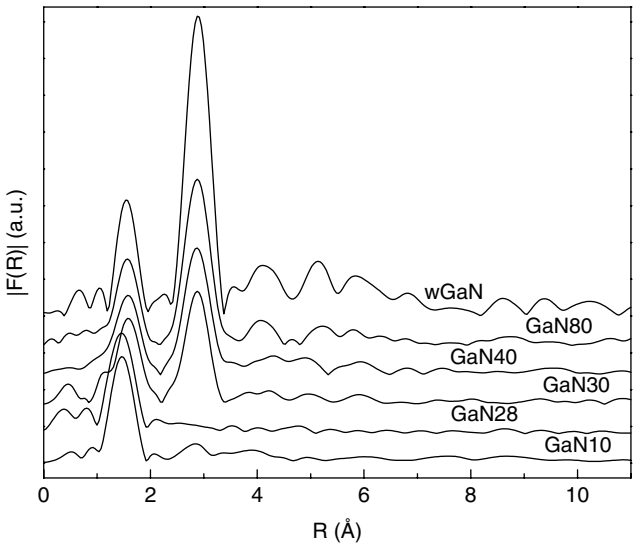

Figure 5. Modulus of the pseudo radial distribution function ($|F(R)|$) (not corrected for phase shift) of GaN10, GaN28, GaN30, GaN40, GaN80 and wGaN, from bottom to top.

deposition times of <50 min on an Si(100) substrate, because the structural disorder of the first Ga–Ga coordination sphere is so high that the second coordination sphere does not contribute to the EXAFS signal. For thicker films, the height of the second shell increases gradually but at its maximum it is half the height of wGaN, which indicates that in all the IAD films the crystalline order is much lower than in the reference sample. Therefore, even for long deposition times (>2 h) the IAD films are highly amorphous on average.

This evolution of the degree of crystallinity can be observed also in the local structural parameters estimated by fitting the experimental and simulated spectra. Despite some of the IAD films having significant amounts of oxygen atoms, the incorporation of one or two oxygen atoms in the first coordination sphere duplicates the number of fit parameters. In addition, almost the same interatomic distances are obtained, with or without oxygen, without improving the reliability of the fitting due to the increase in the number of fit parameters. This is due to the similar behaviour of nitrogen and oxygen atoms as backscatterers. For that reason, oxygen atoms are not taken into account in the following refinement of the structural parameters. On the other hand, because the films are highly amorphous, two different strategies can be adopted to determine the parameters corresponding to each shell of atoms at an average distance R_i: fix the coordination number and look for the width of the shell varying the pseudo Debye–Waller factors (σ_i); or fix σ_i and look for the average coordination numbers. Because coordination numbers are the less accurate structural parameter obtained by EXAFS, the first strategy is used here to obtain the average interatomic distance and the width of the spatial distribution of atoms around R_i. The coordination numbers then were fixed to the ideal hexagonal GaN crystallographic values ($N_1 = 4$, $N_2 = 12$) and the pseudo Debye–Waller factors were refined.

These parameters are listed in Table 3 and experimental (symbols) and simulated (lines) EXAFS and pseudo radial distribution functions are compared in Fig. 6. The fitting

Table 3. First- and second-shell refined parameters of the IAD GaN films and wGaN

	1st shell: Ga–N			2nd shell: Ga–Ga		
	N_1	σ_1 (Å)	R_1 (Å)	N_2	σ_2 (Å)	R_2 (Å)
GaN10	4.0[a]	0.062	1.889	—	—	—
GaN28	4.0[a]	0.062	1.890	—	—	—
GaN30	4.0[a]	0.069	1.944	12.0[a]	0.103	3.176
GaN40	4.0[a]	0.065	1.943	12.0[a]	0.100	3.175
GaN80	4.0[a]	0.066	1.942	12.0[a]	0.090	3.176
wGaN	4.0[a]	0.049	1.938	12.0[a]	0.070	3.175

[a] Fixed parameters.

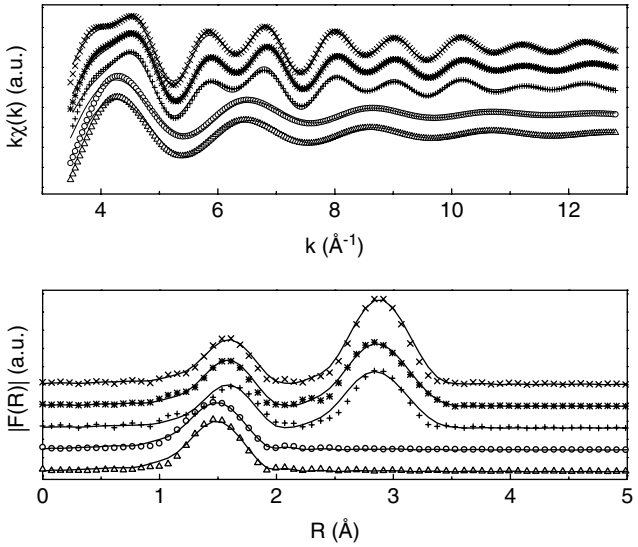

Figure 6. Comparison of experimental (symbols) and simulated (solid lines) modulus of the pseudo radial distribution function (not corrected for phase shift) of the first shell of GaN10 and GaN28 and the first and second shells of GaN30, GaN40, GaN80 and wGaN.

residue was <10% in all cases. Numerical values confirm that the distance of the first coordination sphere (R_1) is slightly shorter in GaN10 and GaN28. As discussed later, this may be due to the higher oxygen occupancy of nitrogen lattice sites in these samples. The second shell of Ga atoms is at 3.176 Å for all the thicker samples, which agrees better with a wurtzite structure (see Table 2). The pseudo Debye–Waller factors of the first shell are very similar for all the films and only slightly higher than that of the reference sample, which suggest that the coordination number is very close to four. However, σ_2 can be used for monitoring the degree of amorphous character of the films. Because the deposition time is longer and the film thickness increases, σ_2 falls from 43% to 25% of the wGaN value, which indicates an evolution of the local crystallographic order towards W-GaN within the studied depth.

Analysis of both the XANES and EXAFS regions thus leads to the same type of conclusions about the evolution of the local structure with film thickness, i.e. thinner films are completely amorphous with Ga atoms tetrahedrally coordinated to N or O atoms, and, at increasing thickness, the average degree of crystallinity increases progressively.

Evolution of the local structure and oxygen content

X-ray absorption at the Ga K-edge has revealed clear differences between the two thinner films ($t_d < 50$ min) and the thicker ones. But GaN10 and GaN28 are also different in chemical composition, because the content of oxygen is as high as 20–25 at.% in these samples and it falls to ~10 at.% in the thicker films. The oxygen content thus seems to be related to the structural properties.

The percentage of oxygen substituting for nitrogen and the long-range crystallographic properties have been correlated in GaN:O films grown by chemical vapour deposition.[25] At a local range, we have some evidence of the substitution of some nitrogen by oxygen in the first coordination sphere of Ga atoms of thinner films, although our results indicate that the tetrahedral configuration of Ga is not significantly modified. It has been reported in the literature that oxygen substitution allows Ga to retain the tetrahedral structure, which is also the low-energy form of Ga–O bonds in gallium oxide.[25,48] The percentage of N substitution can be as high as 50% (25 at.% of oxygen) and the only difference between Ga–O and Ga–N tetrahedra is the shorter interatomic distance of Ga–O (1.82 Å vs. 1.94 Å for Ga–N). As pointed out above, we have observed a decrease of the interatomic distance of the first coordination sphere around Ga atoms in GaN10 and GaN28 (Table 3). Because the oxygen percentage of these two films is higher, this shift seems to be related to the higher oxygen occupancy of nitrogen lattice sites in these samples. Further chemical analysis by ion mass spectrometry and XPS are planned to elucidate the possible correlation between structure and oxygen impurities of the IAD GaN films.

On the other hand, in our IAD GaN films, TEM has shown two distinct layers in a film ~190 nm thick deposited on quartz:[16] the layer in contact with the substrate is 120 nm thick and is amorphous, whereas the top layer (~70 nm thick) shows spots of 7–10 nm that may correspond to GaN nanocrystallites. This layered arrangement can be deduced also by comparison of TEY (surface sensitivity) and transmission (bulk sensitivity) x-ray absorption results. In a previous transmission EXAFS experiment carried out on a 1000 nm thick film deposited onto Mylar,[13] the height of the $|F(R)|$ peak corresponding to the second shell was one-third of the height of wGaN measured in transmission mode, whereas the first shell showed almost the same intensity for both samples. In TEY, the height of the second $|F(R)|$ peak for the thickest film (~450 nm) is half that of the reference sample. Because in the transmission experiments all the film contributes to the EXAFS signal and in TEY EXAFS the outer surface layer is preferentially probed, XAFS also supports the existence of a gradient of crystallinity from the surface to the bulk of IAD GaN films that are thick enough.

Because oxygen impurities seem to be related to crystallographic properties, at this stage we think that this layered arrangement is due to a decrease in the amount of water vapour in the chamber as the GaN is growing, although it could be due to heating of the film by the ion beam for long

deposition times or to differences in substrate crystallinity. Assuming that the presence of oxygen in the deposition chamber decreases with the deposition time, the bad correlation between optical thickness and deposition time of GaN10, GaN28 and GaN30 can be explained because the growth rate depends on the partial pressure of water inside the chamber. Above a certain threshold, most of the oxygen is exhausted and the growth rate may change suddenly.

CONCLUSIONS

X-ray absorption spectroscopy at the Ga K-edge has been used to study the short-range order of a series of GaN : O films grown by IAD at increasing deposition times on a silicon substrate. No evidence of separate gallium oxide or metallic gallium has been found. Results have shown that Ga atoms are predominantly tetrahedrally coordinated to nitrogen atoms, some of which could be substituted by oxygen. Films grown for <50 min are fully amorphous: dispersion of Ga–Ga distances is so high that the first sphere of coordination of Ga atoms is not observed by EXAFS. Despite the high oxygen content of these films, they may exhibit exploitable optoelectronic properties.[16]

Films grown for longer times have shown certain order in the first Ga–Ga coordination sphere, but bonding distortions are always higher than in a polycrystalline GaN sample. Neighbouring Ga atoms at ~3.18 Å are first observed by EXAFS for a GaN film 260 nm thick after 50 min of deposition time. As the deposition time increases, the distribution of Ga–Ga distances narrows, which indicates a gradual increase of local order within the studied depth (<100 nm).

Comparing the results of transmission and TEY x-ray absorption, the higher crystalline local order seems to be localized in the outer surface of the thicker film, which agrees with a layered distribution of GaN crystallinity. Above a certain thickness (or deposition time), nanocrystalline GaN begins to grow on the top of the amorphous GaN : O layer. The transition from amorphous to nanocrystalline seems to be related to a decrease in the oxygen available inside the deposition chamber as the film grows. In nanocrystalline films, the size of the crystal domains remains below 3 nm for all the studied samples, and the ratio of crystallites to amorphous network increases gradually with deposition times in a top surface layer ~100 nm thick.

Acknowledgements

We are grateful to the Laboratoire pour Utilisation du Rayonnement Electromagnétique for beam time. We also thank John Kennedy for RBS data. M.J.A. thanks the Spanish government (MCyT, Ramon y Cajal program) for financial support.

REFERENCES

1. Stumm P, Drabold DA. *Phys. Rev. Lett.* 1997; **79**: 677.
2. Yu M, Drabold DA. *Solid State Commun.* 1998; **108**: 413.
3. Mott NF, Davis EA. *Electronic Processes in Non-Crystalline Materials* (2nd edn). Clarendon Press: Oxford, 1979.
4. Zallen R. *The Physics of Amorphous Solids*. John Wiley: New York, 1983.
5. Yang Y, Leppert VL, Risbud SH, Twamley B, Power PP, Lee HWH. *Appl. Phys. Lett.* 1999; **74**: 2262.
6. Kuball M, Mokhtari H, Cherns D, Lu J, Westwood DI. *Jpn. J. Appl. Phys. Part I* 2000; **39**: 4753.
7. Chen H, Chen K, Drabold DA, Kordesch ME. *Appl. Phys. Lett.* 2000; **77**: 1117.
8. Preschilla N, Major S, Kumar N, Samajdar I, Srinivasa RS. *Appl. Phys. Lett.* 2000; **77**: 1861.
9. Bittar A, Trodahl HJ, Kemp NT, Markwitz A. *Appl. Phys. Lett.* 2001; **78**: 619.
10. Miyazaki T, Fujimaki T, Adachi S, Ohtsuka K. *J. Appl. Phys.* 2001; **89**: 8316.
11. Yamada K, Asahi H, Tampo H, Imanishi Y, Ohnishi K, Asami K. *Appl. Phys. Lett.* 2001; **78**: 2849.
12. Lanke UD, Koo A, Granville S, Trodahl HJ, Markwitz A, Kennedy VJ, Bittar A. *Mod. Phys. Lett. B* 2001; **15**: 1355.
13. Lanke UD, Koo A, Ruck BJ, Lee HK, Markwitz A, Kennedy VJ, Ariza MJ, Jones DJ, Rozière J, Bittar A, Trodahl HJ. *Mater. Res. Soc. Symp. Proc.* 2002; **693**: 347.
14. Koo A, Lanke UD, Ruck BJ, Brown S, Reeves R, Bittar A, Trodahl HJ. *Mater. Res. Soc. Symp. Proc.* 2002; **693**: 621.
15. Metson JB, Trodahl HJ, Ruck BJ, Lanke UD, Bittar A. *Surf. Interface Anal.* 2003; **35**: 719.
16. Koo A, Ruck BJ, Lanke UD, Metson JB, Ariza MJ, Jones DJ, Rozière J, Bittar A, Trodahl HJ. *Proc. 26th International Conference on the Physics of Semiconductors*. Institute of Physics Publishing: Bristol, 2003.
17. Kang Y, Ingram DC. *J. Appl. Phys.* 2003; **93**: 3954.
18. Nonomura S, Kobayashi S, Gotoh T, Hirata S, Ohmori T, Itoh T, Nitta S, Morigaki K. *J. Non-Cryst. Solids* 1996; **198–200**: 174.
19. Kobayashi S, Nonomura S, Ohmori T, Abe K, Hirata S, Uno T, Gotoh T, Nitta S. *Appl. Surf. Sci.* 1997; **113/114**: 480.
20. Silva SRP, Almeida SA, Sealy BJ. *Nucl. Instrum. Methods Phys. Res. B* 1999; **147**: 388.
21. Kench PJ, Shannon JM, Shao G, Tsakiropoulos P, Silva SRP. *Nucl. Instrum. Methods Phys. Res. B* 2001; **175–177**: 678.
22. Oila J, Ranki V, Kivioja J, Saarinen K, Hautojarvi P, Likonen J, Baranowski JM, Pakula K, Suski T, Leszczynski M, Grzegory I. *Phys. Rev. B* 2001; **63**: 045 205.
23. Korotkov RY, Niu F, Gregie JM, Wessels BW. *Phys. B* 2001; **308–310**: 26.
24. Aleksandrov SE, Gavrikova TA, Zykov VA. *Semiconductors* 2000; **34**: 291.
25. Tran NH, Holzschuh WJ, Lamb RN, Lai LJ, Yang YW. *J. Phys. Chem. B* 2003; **107**: 9256.
26. Budde F, Ruck BJ, Koo A, Granville S, Trodahl HJ, Bittar A, Williams GVM, Ariza MJ, Bonnet B, Jones DJ, Metson JB, Rubanov S, Munroe P. *Phys. Rev. B.* (Submitted).
27. Hirvonen JK. *Mater. Sci. Rep.* 1991; **6**: 215.
28. Kennedy VJ, Markwitz A, Lanke UD, McIvor A, Trodahl HJ, Bittar A. *Nucl. Instrum. Methods Phys. Res. B* 2002; **190**: 620.
29. Koningsberger DC, Prins R. *X-ray Absorption: Principles, Applications, Techniques of EXAFS, SEXAFS and XANES*. John Wiley: New York, 1988.
30. Stern EA, Ma Y, Hanske-Petitpierre O, Bouldin CE. *Phys. Rev. B* 1992; **46**: 687.
31. Stern EA, Livins P, Zhang Z. *Phys. Rev. B* 1991; **43**: 8850.
32. Perlin P, Jauberthie-Carillon C, Itie JP, San Miguel A, Grzegory I, Polian A. *Phys. Rev. B* 1992; **45**: 83.
33. Katsikini M, Rossner H, Fieber-Erdmann M, Holub-Krappe E, Moustakas TD, Paloura EC. *J. Synchr. Radiat.* 1999; **6**: 561.
34. Lawniczak-Jablonska K, Iwanowski RJ, Demchenko IN, Boettcher T, Einfeldt S, Hommel D, Cortes R, Perera RCC. *J. Alloys Compounds* 2001; **328**: 77.
35. Li Z, Wei S, Wang Y, Zhang X, Lu K, Chen X. *J. Synchr. Radiat.* 2001; **8**: 830.
36. Erbil A, Cargill III GS, Frahm R, Boehme RF. *Phys. Rev. B* 1988; **37**: 2450.
37. Traverse A, Parent P, Mimault J, Hagège S, Du J. *Nucl. Instrum. Methods Phys. Res. Sect. B* 1994; **84**: 204.
38. Jiménez VM, Caballero A, Fernandez A, Sanchez-Lopez JC, Gonzalez-Elipe AR, Trigo JF, Sanz JM. *Surf. Interface Anal.* 1997; **25**: 707.

39. Trodahl HJ, Ruck BJ, Lanke UD, Granville S, Budde F, Koo A, Bittar A. *Phys. Rev. B.* (Submitted).
40. Ruck BJ, Koo A, Lanke UD, Budde F, Granville S, Trodahl HJ, Bittar A, Kennedy VJ, Markwitz A. *Phys. Rev. B.* (Accepted).
41. Mimault J, Faix JJ, Girardeau T, Jaouen M, Tourillon G. *Meas. Sci. Technol.* 1994; **5**: 482.
42. Michalowicz A. *Logiciels pour la Chimie*. Société Française de Chimie: Paris, 1991.
43. McKale AG, Veal BW, Paulikas AP, Chan SK, Knapp GS. *J. Am. Chem. Soc.* 1988; **110**: 3763.
44. Wright AF, Nelson JS. *Phys. Rev. B* 1994; **50**: 2159.
45. Juza R, Hahn H. *Z. Anorg. Allg. Chem.* 1938; **239**: 282.
46. *RETRIEVE, Inorganic Crystal Structure Database (ICSD)*, Gmelin Institute & FIZ Karlsruhe: Eggenstein-Leopoldshafen, Germany, 2000; Fluck E. *J. Res. Natl. Inst. Stand. Technol.* 1996; **101**: 217.
47. Katsikini M, Paloura EC, Fieber-Erdmann M, Kalomiros J, Moustakas TD, Amano H, Akasaki I. *Phys. Rev. B* 1997; **56**: 13 380.
48. Nishi K, Shimizu K, Takamatsu M, Hisao Y, Satsuma A, Tanaka T, Yoshida S, Hattori T. *J. Phys. Chem. B* 1998; **102**: 10 190.
49. Dalba G, Diop D, Fornasini P, Kuzmin A, Rocca F. *J. Phys.: Condens. Matter* 1993; **5**: 1643.